Geophysical Research Letters

RESEARCH LETTER
10.1029/2023GL103515

Deconstructing Future AMOC Decline at 26.5°N

Helene Asbjørnsen[1,2] and **Marius Årthun**[1,2]

[1]Geophysical Institute, University of Bergen, Bergen, Norway, [2]Bjerknes Centre for Climate Research, Bergen, Norway

Key Points:

- Future Atlantic Meridional Overturning Circulation decline is deconstructed by quantifying changes in the Gulf Stream, Deep Western Boundary Current (DWBC), and gyre recirculation
- In a high emission scenario, Coupled Model Intercomparison Project Phase 6 models show a Gulf Stream weakening of 29% and a DWBC weakening of 47% at 26.5°N by the end of the century
- 33% of the Gulf Stream weakening is due to changes in winds

Supporting Information:

Supporting Information may be found in the online version of this article.

Correspondence to:

H. Asbjørnsen,
h.asbjornsen@uib.no

Citation:

Asbjørnsen, H., & Årthun, M. (2023). Deconstructing future AMOC decline at 26.5°N. *Geophysical Research Letters*, *50*, e2023GL103515. https://doi.org/10.1029/2023GL103515

Received 14 MAR 2023
Accepted 5 JUN 2023

Abstract The Atlantic Meridional Overturning Circulation (AMOC) is frequently used to diagnose the state of the North Atlantic circulation, but as an integrated quantity the AMOC strength does not necessarily mirror changes in the individual circulation components. Here, we investigate future circulation changes in the subtropical North Atlantic (26.5°N) in CMIP6 models, diagnosing the relationship between the Gulf Stream, Deep Western Boundary Current (DWBC), gyre recirculation, and the integrated AMOC response. Under continued high emissions, we find a multi-model mean Gulf Stream weakening of 29% (11.2 Sv) and a DWBC weakening of 47% (8.5 Sv) by the end of the century. However, 33% (3.7 Sv) of the Gulf Stream weakening is due to changes in wind stress and therefore not simply a compensating effect for reduced high-latitude water mass transformation and a weaker DWBC. Our findings have implications for how we understand the dynamics of future North Atlantic circulation changes.

Plain Language Summary Climate models show circulation in the North Atlantic Ocean to weaken under continued high greenhouse gas emissions. How this weakening is expressed in the Gulf Stream, Deep Western Boundary Current (DWBC), and subtropical gyre circulation remains little explored. Here, we use models that contributed to the Coupled Model Intercomparison Project Phase 6 to investigate potential future changes in the subtropical North Atlantic Ocean. Averaging over 14 models, we find the Gulf Stream to weaken by 29% and the DWBC to weaken by 47% by the end of the century. As much as 33% of the Gulf Stream weakening is due to changes in the large-scale winds, while the remaining fraction is compensating for the weakening DWBC. Our findings have implications for understanding the interconnectedness of the different circulation branches and their relationship to the large-scale Atlantic Meridional Overturning Circulation.

1. Introduction

Future global warming is projected to cause substantial changes in the ocean circulation manifested in poleward shifted ocean gyres (Yang et al., 2020), retreating sea ice (e.g., Årthun et al., 2021), shift in dense water formation sites (e.g., Bretones et al., 2022; Lique & Thomas, 2018), and a weakening North Atlantic circulation (e.g., Weaver et al., 2012; Weijer et al., 2020). North Atlantic circulation strength is typically diagnosed by the strength of the Atlantic Meridional Overturning Circulation (AMOC), which quantifies the net upper-ocean northward flow with an equally large southward return flow at depth and thus represents the amount of water that "overturns" at high latitudes. Past and future changes in the AMOC are, however, poorly understood and remains a source of uncertainty in CMIP-class climate models (Bellomo et al., 2021; Robson et al., 2022; Swingedouw et al., 2022).

In the subtropical North Atlantic, the Gulf Stream transports warm water northward while the Deep Western Boundary Current (DWBC) transports North Atlantic Deep Water (NADW) southward at depth. The AMOC strength measured at the RAPID-MOCHA-WBTS array at 26.5°N since 2004 (Cunningham et al., 2007; Moat et al., 2020) provides a valuable reference for evaluating North Atlantic circulation in climate models. At 26.5°N, the Florida Current and the Antilles Current mark the start of the Gulf Stream (Baringer & Larsen, 2001; Meinen et al., 2019) with the DWBC east of the continental shelf (Biló & Johns, 2020). Prevailing zonal winds set up the subtropical gyre circulation by inducing a net southward transport over the mid-basin that is compensated at the western boundary (Sverdrup, 1947). Analyzing transports across 26.5°N is ideal for "taking the pulse" of the climate system as it reflects both wind-driven gyre dynamics, dense water in the DWBC formed north of the section, and the overall heat being transported from the subtropics toward the Arctic.

The current generation of CMIP models shows no systematic AMOC decline over the historical period (Menary et al., 2020), but projects a weakening circulation over the 21st century (Weijer et al., 2020). The AMOC is, however, an integrated quantity masking the full three-dimensional flow (Roquet & Wunsch, 2022) and reflects a

multitude of changes related to both wind and buoyancy forcing (e.g., Lozier, 2012). Changes in individual North Atlantic circulation branches and how they project onto a weakening AMOC remain little explored, though is key for understanding the mechanisms of future change. If the total Gulf Stream transport remains fixed, a strengthened gyre implies a weakened AMOC as the difference between the northward Gulf Stream and southward gyre recirculation is reduced (Wunsch & Heimbach, 2013). However, some model studies find a stronger AMOC to be associated with a strengthened gyre, indicating that the same mechanisms strengthening the wind-driven gyre also strengthen the buoyancy-driven part of the Gulf Stream (de Coëtlogon et al., 2006; Larson et al., 2020). The North Atlantic Oscillation (NAO) has been proposed as a mechanism that can drive wind and buoyancy anomalies on similar time scales (Eden & Willebrand, 2001). In the deep ocean, most of the transport is carried by the southward DWBC. However, time-variable, deep northward recirculations have the potential to limit the co-variance between the DWBC and the AMOC strength (Biló & Johns, 2020; Kanzow et al., 2008). As a result, inferences about changes in the Gulf Stream, DWBC, and gyre strength cannot necessarily be made directly from the evolution of the AMOC.

In this study we accordingly investigate changes in the Gulf Stream and DWBC, and their relationship to the AMOC and the gyre recirculation under continued high greenhouse gas emissions. We use CMIP6 models to objectively identify the Gulf Stream, DWBC, and gyre recirculation from the velocity field and diagnose the projected changes by the end of the 21st century at 26.5°N. We apply Sverdrup theory to infer changes in the subtropical gyre, and thus also the Gulf Stream, from changes in the wind stress. The results show a future subtropical North Atlantic characterized by weaker, warmer, and saltier western boundary currents compared to today.

2. Methods

To assess potential future change in the circulation at 26.5°N we analyze a selection of CMIP6 models (Table S1 in Supporting Information S1). The models were selected based on availability of monthly meridional ocean velocity and mass transport (model variables vo and vmo). We use the CMIP6 historical simulations (Eyring et al., 2016; here 1920–2014) as a historical reference for the models. However, we focus our analysis on the Shared Socioeconomic Pathways (SSP, Gidden et al., 2019) scenario SSP5-8.5 ("ssp585") representing a high-emission scenario. For the circulation strength across 26.5°N, we analyze 14 models (Table S1 in Supporting Information S1). For the analysis requiring the surface wind stress only 10 of the models had the necessary variables (tauuo, tauvo; surface wind stress on the ocean grid) available. We extract the fields at the individual model's native grid line closest to 26.5°N, which leads to small (under 0.5°) differences in latitude between the model sections analyzed. Prior to analysis, we compute annual means of the monthly mean output fields.

As a first check, we test whether the models uphold mass-balance at 26.5°N. Due to the net inflow through the Bering Strait of 0.9 ± 0.1 Sv (Østerhus et al., 2019), a net southward transport of approximately 1 Sv is expected at 26.5°N. All the models have a mean net southward transport of roughly 1 Sv for the historical period (Figure S1 in Supporting Information S1). However, the MIROC6 model has a larger standard deviation than the other models, and displays a trend in the net transport across the section during the ssp585 scenario. The trend is, in-part, related to a weakening inflow through the Bering Strait in MIROC6 (roughly 0.5 Sv reduction between 2030 and 2100).

The Gulf Stream and the DWBC at 26.5°N are identified from the velocity field by detecting the high velocity cores at the western boundary. In order to define the Gulf Stream and DWBC cores within each model, we find the upper-ocean northward velocity maxima (0–1,100 m; $v_{N_{\max}}$) and lower-ocean southward velocity maxima (>1,100 m; $v_{S_{\max}}$) at each time step. Grid cells in the upper-ocean with a velocity greater than 5% of $v_{N_{\max}}$ are identified as being a part of the Gulf Stream core. Equivalently, grid cells with a velocity greater than 5% of $v_{S_{\max}}$ in the lower-ocean are a part of the DWBC core. Apart from the higher resolution MPI-ESM1-2-HR model ($0.4° \times 0.4°$ nominal resolution), the models do not resolve the Antilles Current as a separate branch from the Florida Current (Figure S2 in Supporting Information S1). We therefore remove high velocity points detached from the western boundary cores for all models expect MPI-ESM1-2-HR. The integrated transport magnitudes within the cores are not sensitive to the exact cut-off percentage used (here 5%) as long as a value below 10% is chosen. We use 1,100 m as the maximum depth of the northward flowing Gulf Stream at 26.5°N because the typical depth of the maximum overturning stream function in observations from RAPID is 1,100 m (Figure S3 in Supporting Information S1). The results show no sensitivity to the exact choice of the depth criteria, testing

for values between 1,000 and 1,200 m. The core detection method is independent of the model grid, and avoids using water mass definitions as there are known biases in the properties of for instance NADW in CMIP6 models (Heuzé, 2021). The method also allows for the structure of the high velocity cores to vary between models and to evolve over time within a single model. After defining the Gulf Stream and DWBC cores, the residual flow is defined as the "gyre recirculation" component which is characterized by weaker velocities in the mid-ocean basin (Figure S2 in Supporting Information S1).

Using our core detection method, the multi-model mean shows a 39.3 Sv Gulf Stream transport for the historical period compared to the approximately 37 Sv for the Florida Current and the Antilles Current combined in observations (Baringer & Larsen, 2001; Meinen et al., 2019). While the multi-model mean compares very well, we note that there are models with a too strong (e.g., EC-Earth3) and too weak Gulf Stream (e.g., MRI-ESM2-0) compared to observations (Figure S4 in Supporting Information S1). The RAPID estimate indicates a net southward NADW transport of 17.8 Sv (Bryden, 2021), which is comparable to the multi-model mean DWBC transport of 18.9 Sv. Moorings in the DWBC (2008–2018) shows, however, an average transport of 28.3 Sv (Biló & Johns, 2020), indicating that there is a sizeable northward recirculation of NADW offshore of the DWBC that is not fully captured by the CMIP6 models.

For further diagnostics, we calculate the AMOC strength and the Sverdrup transport at 26.5°N. The AMOC strength is defined as the maximum of the overturning stream function in depth-space:

$$moc_z = \max\left[\int_0^z \int_{x_w}^{x_e} v(x,z)\,dx\,dz\right] \tag{1}$$

The zonally integrated Sverdrup transport is calculated from the surface wind stress on the ocean grid as:

$$V_{sverd} = \frac{1}{\rho_0 \beta}\int_{x_{gs}}^{x_e}\left(\frac{\partial \tau_y}{\partial x} - \frac{\partial \tau_x}{\partial y}\right)dx \tag{2}$$

When zonally integrating to obtain the net Sverdrup transport across the section (V_{sverd}), we integrate from the first grid cell east of the identified Gulf Stream core (x_{gs}) to the eastern boundary (x_e). This excludes the western boundary region where Sverdrup balance is not valid (e.g., Thomas et al., 2014). At 26.5°N, V_{sverd} is directed southward as the negative (anticyclonic) wind stress curl in the subtropics causes Ekman pumping which stretches the water column and induces equatorward motion. According to Sverdrup theory, V_{sverd} represents the mid-ocean, wind-driven gyre circulation assuming that a level of no motion exists above which circulation is purely wind-driven (Sverdrup, 1947).

3. Results

Mass conservation at 26.5°N under projected circulation slowdown requires a balance between changes in the Gulf Stream, DWBC, and the gyre recirculation (e.g., Bryden, 2021). For instance, if the DWBC weaken due to reduced NADW formation rates north of 26.5°N, the Gulf Stream must weaken and/or the gyre recirculation must strengthen for mass to be conserved (Figure 2a). Likewise, a weakened gyre circulation due to reduced wind stress curl will be reflected by both a weakened southward mid-ocean transport (here, the gyre recirculation) and a weakened Gulf Stream at the western boundary. Changes in the various components will project onto the AMOC (Figure 1a).

While the simulated branches display a stable transport over the historical period, we find the Gulf Stream, DWBC, and the gyre recirculation to weaken under ssp585 (Figures 1b–1d). For the future scenario, the Gulf Stream weakens by 29% (11.2 Sv, inter-model spread 20%–50%) and the DWBC weakens by 47% (8.5 Sv, inter-model spread 22%–71%) comparing the 2015–2025 decade to the 2090–2100 decade (Figure 2b). The gyre recirculation component shows a weakening of 12% (2.7 Sv, inter-model spread −4%–33%), indicative of a weakened subtropical gyre.

To determine whether the weakening gyre recirculation reflects changes in wind forcing, we calculate the Sverdrup transport across 26.5°N from the surface wind stress (Equation 2). The Sverdrup transport magnitude seen in Figure 2b is close to that of the gyre recirculation component, demonstrating that the gyre recirculation (defined as a residual) reflects the wind-driven gyre to a large extent. An 18% (3.7 Sv, inter-model spread

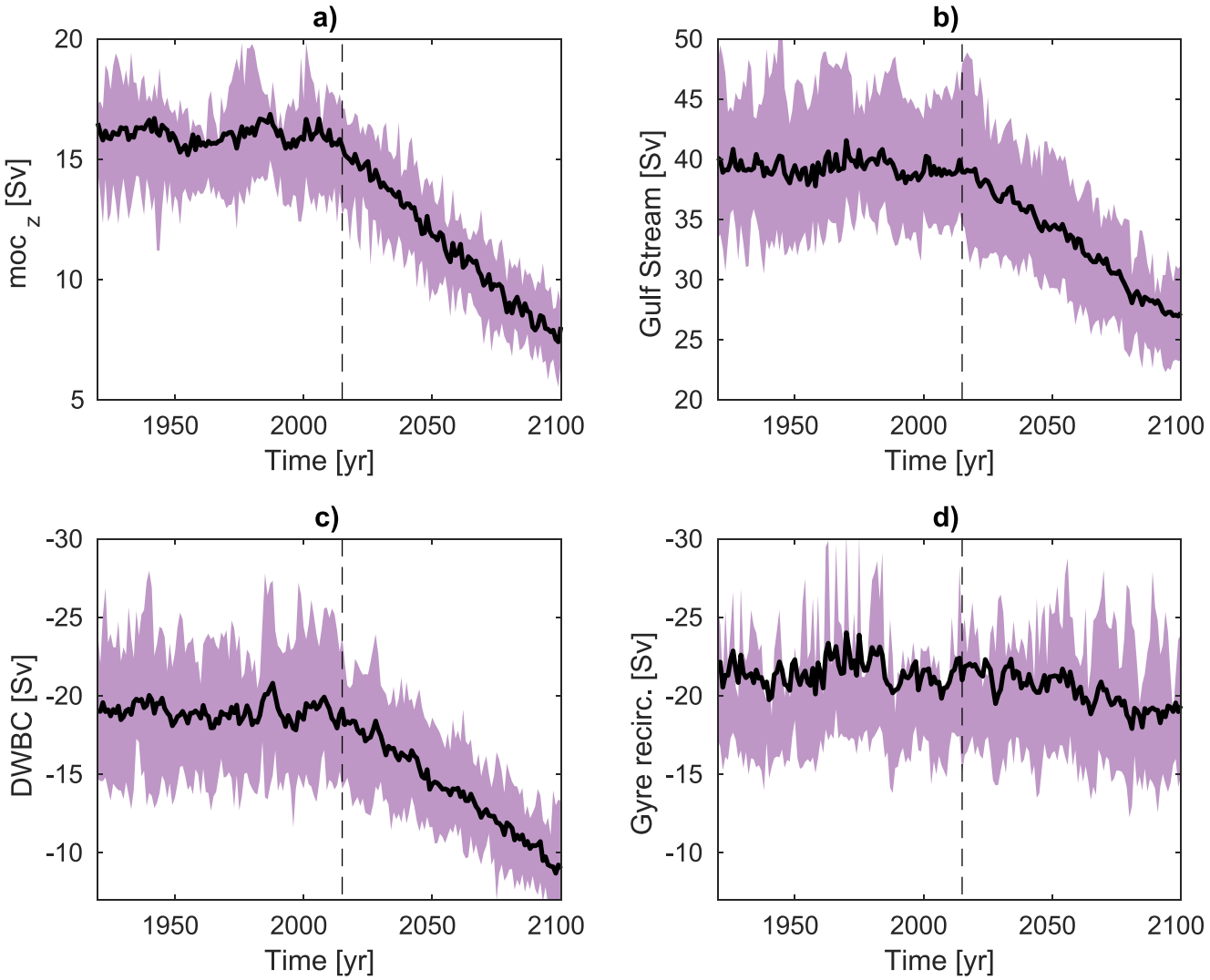

Figure 1. Multi-model mean transports at 26.5°N of 14 CMIP6 models with historical forcing (1920–2014) and the ssp585 emission scenario (2015–2100). (a) AMOC strength, (b) Gulf Stream transport, (c) Deep Western Boundary Current (DWBC) transport, and (d) gyre recirculation defined as the residual flow. Shading shows the interquartile range. The dashed line shows the start of the ssp585 projection. Positive/negative transport values denote northward/southward flow. The *y*-axes in (c, d) are flipped to illustrate the weakening in the components with a mean net southward transport. Also note the different limits on the *y*-axes. In (d), the skewness of the multi-model mean compared to the spread is due to the strong gyre in the CNRM-ESM2, EC-Earth3, and IPSL-CM6A-LR models.

6%–25%) weakening in the Sverdrup transport moreover indicate that the weakening in the gyre recirculation component is due to changes in the wind stress curl. Given that Sverdrup balance holds, changes in the Sverdrup transport are compensated at the western boundary in the Gulf Stream. With a multi-model mean Gulf Stream weakening of 11.2 Sv and a Sverdrup transport weakening of 3.7 Sv, this implies that as much as 33% of the Gulf Stream weakening by the end of the century is explained by changes in the wind stress.

Changes in the large-scale winds contributing to weakening the circulation is consistent with Thomas et al. (2012) who, in a 100-year climate model integration with an annual 2% CO_2 increase for the first 70 years, get a reduced Sverdrup transport at 26.5°N. Beadling et al. (2018) also find a weakening Sverdrup transport with reduced subtropical wind stress curl in 14 of 15 CMIP5 models, ranging between 8% and 33% reduction (first vs. last 20-years of RCP8.5). Changes in the wind stress curl can be related to a weaker, poleward expanded Hadley cell and poleward shifted westerlies under global warming (Grise & Davis, 2020; Harvey et al., 2020; Lu et al., 2007).

Looking at the relative strength of the different circulation components, the AMOC strength consistently scale with the DWBC strength across all models analyzed (Figure 3b; $r_{mm} = -0.80$). The relationship between the

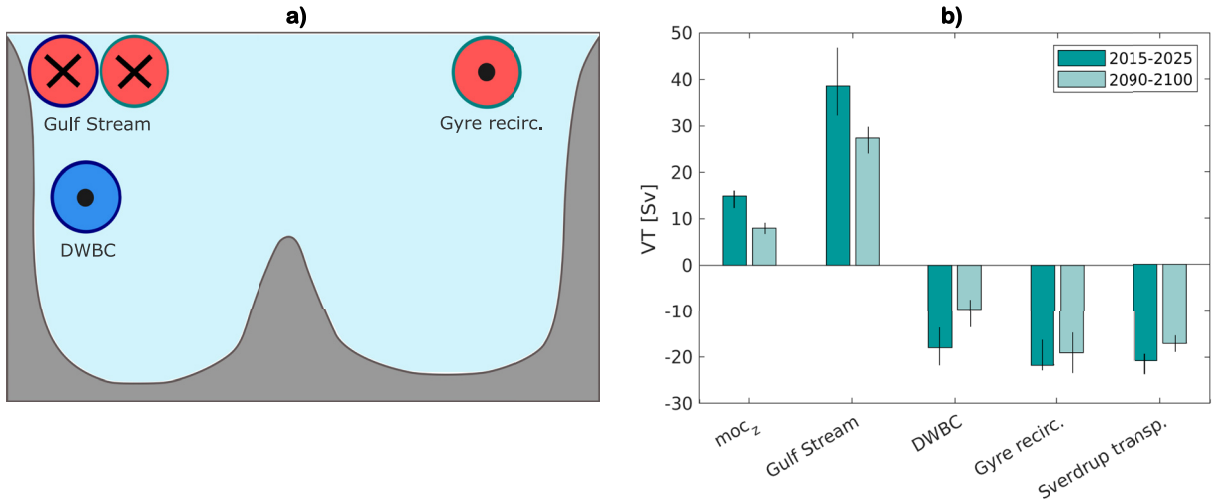

Figure 2. Mass-balance at 26.5°N. (a) Schematic illustrating idealized mass-balance between the three components. The red circles indicate the warm, upper-ocean components and the blue circle the colder deep component. The Gulf Stream is shown using two circles highlighting it partly compensating for the DWBC, partly being the western boundary of the subtropical gyre. (b) Multi-model mean transports at 26.5°N of 14 CMIP6 models under the ssp585 emission scenario (first vs. last decade). Whiskers show the interquartile range. The multi-model mean Sverdrup transport is calculated from wind stress, and is averaged over 10 models (Table S1 in Supporting Information S1).

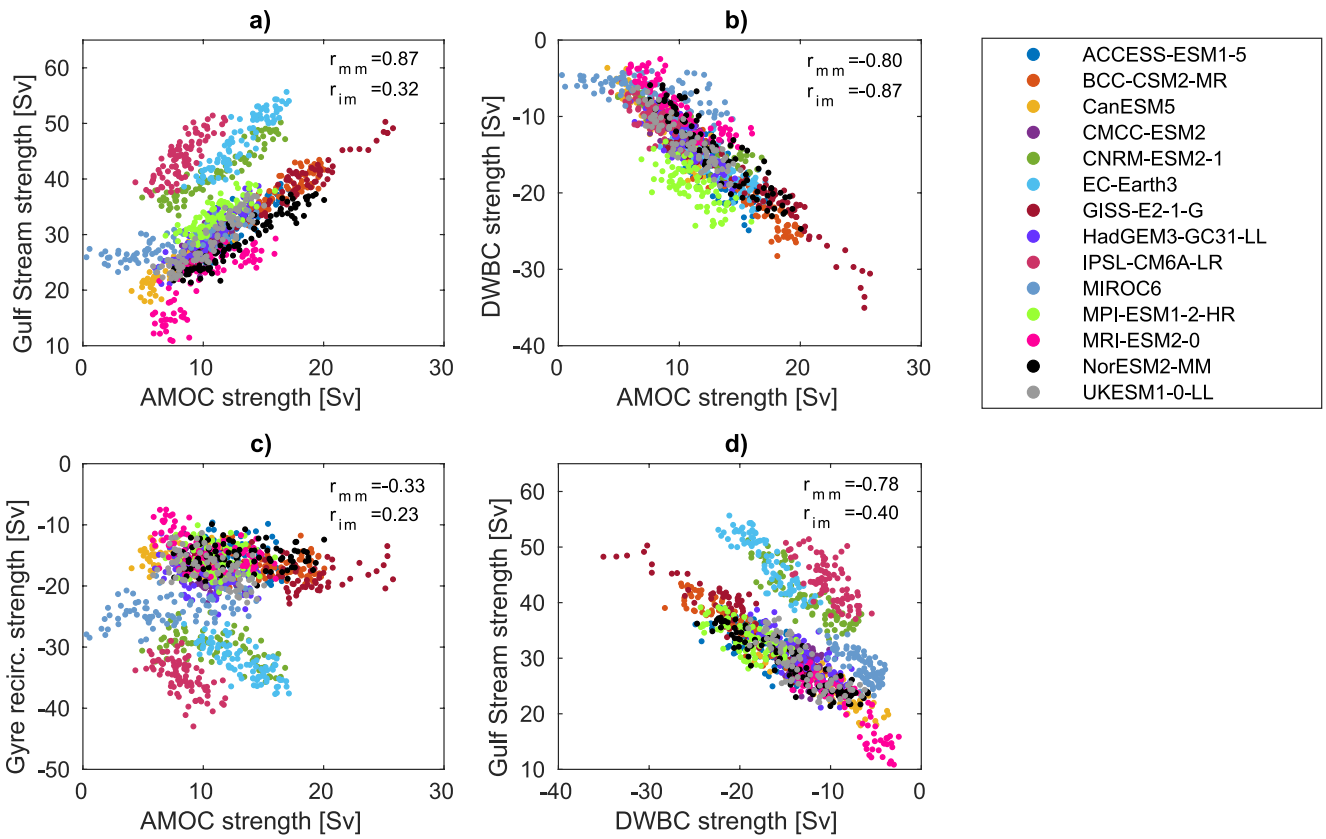

Figure 3. Relative strength between circulation components at 26.5°N. (a–c) Relative strength of the AMOC and the Gulf Stream, DWBC, and gyre recirculation, respectively, for each year (2015–2100) in the ssp585 emission scenario in the 14 models analyzed. (d) As (a–c), but showing the relative strength between the DWBC and the Gulf Stream. The multi-model mean correlation (r_{mm}; average correlation across models) and the inter-model correlation (r_{im}; correlation between the 14 models' mean transport values) coefficients are shown in the panels' upper-right corner.

Gulf Stream and the AMOC strength also approximately scales linearly (Figure 3a; $r_{mm} = 0.87$), but shows larger inter-model differences in the Gulf Stream magnitude relative to the AMOC magnitude ($r_{im} = 0.32$) due to differences in the climatological upper-ocean circulation. For instance, the three models clustering in Figure 3a (CNRM-ESM2, EC-Earth3, and IPSL-CM6A-LR) all have a strong gyre recirculation and a strong, narrow Florida Current in the Florida Straits with no representation of the Antilles Current further offshore (Figures S2 and S4 in Supporting Information S1).

There are also inter-model differences in the relationship between the gyre recirculation and the AMOC (Figure 3c). We find that 10 of the models have a significant (at the 95% confidence level) "weak gyre-weak AMOC" relationship similar to what was indicated in Larson et al. (2020). Three models have no significant relationship (CanESM5, MPI-ESM1-2-HR, NorESM2-MM), and one model have a significant "strong gyre-weak AMOC relationship" (MIROC6). The majority of the models showing a "weak AMOC-weak gyre" link means that there is a tendency for both the wind-driven (gyre component) and buoyancy-driven part of the Gulf Stream to weaken on similar time scales so that the net upper-ocean northward transport across 26.5°N reduces, thus weakening the AMOC.

In addition to weakened transports, CMIP6 models also show future changes in the thermohaline properties of the Gulf Stream and the DWBC. We find a temperature-driven reduction in NADW densities as both the Gulf Stream source water and the DWBC get warmer and saltier (Figure 4). The shoaling of the overturning stream function maximum by the end of the century seen in Figure S3 of the Supporting Information S1 is consistent with NADW getting lighter. A warmer, saltier DWBC is consistent with Levang and Schmitt (2020) showing that the weakening geostrophic component of the AMOC in CMIP5 models is driven by temperature anomalies in the 1,000–2,000 m depth layer rather than freshwater anomalies. This does, however, not exclude increased stratification from surface freshening in the subpolar North Atlantic (SPNA) from having an important role, as reduced mixing with cold surface water in the SPNA can contribute to warming the NADW. Despite the increasing Gulf Stream temperatures, the heat transported from the subtropics is projected to reduce due to the weakened circulation strength. Across 26.5°N, we find the net northward heat transport to reduce by 37% (0.3 PW) by the end of the 21st century (Figure S5 in Supporting Information S1).

4. Discussion and Conclusions

Investigating the different circulation branches that combined make up the AMOC at 26.5°N in CMIP6 models, we have diagnosed future North Atlantic circulation change under continued high-emissions. We find that all three components—the Gulf Stream, the DWBC, and the gyre recirculation—weaken over the 21st century. As the weakening gyre recirculation reflects changes in the surface wind stress, this implies that parts of the Gulf Stream weakening is due to changes in atmospheric circulation. We find that 33% of the Gulf Stream weakening in CMIP6 models is caused by changes in the wind stress curl (Figure 2b), with the remaining fractional Gulf Stream weakening compensating for reduced DWBC transport. The Gulf Stream weakening at 26.5°N identified here (29% reduction) is larger than what was reported by Sen Gupta et al. (2021) based on CMIP5 and CMIP6 models (15% reduction in 2050–2100 relative to 1900–2000). We note, however, that differences in the Gulf Stream definition and reference period will give somewhat different fractional reductions.

A weakening DWBC (47%; first vs. last decade of ssp585) is consistent with reduced NADW formation rates as a result of changes in high latitude buoyancy fluxes (e.g., Levang & Schmitt, 2020; Maroon et al., 2018). Based on CMIP5 models, Beadling et al. (2018) find a 28% weakening of the net deep ocean transport, that is, not just the DWBC, at 26.5°N (first vs. last 20-years of RCP8.5). Using an equivalent deep ocean transport definition as that in Beadling et al. (2018), we find a 38% multi-model mean weakening (first vs. last 20-years of ssp585) which is still notably higher than for the CMIP5 models.

Our analysis shows the AMOC strength to scale with the DWBC strength with an approximate linear relationship across and between the different CMIP6 models, confirming a model-independent proxy relationship between the two under projected climate change (Figure 3b). Such a relationship between the AMOC strength and DWBC strength likely is, however, somewhat stronger in CMIP6 simulations than in nature because of the limited deep recirculation in the models.

Several processes important for the AMOC, such as dense water overflows (Heuzé & Årthun, 2019), deep convection (Heuzé, 2021), transport of freshwater (Swingedouw et al., 2022), and position of the Gulf Stream and North

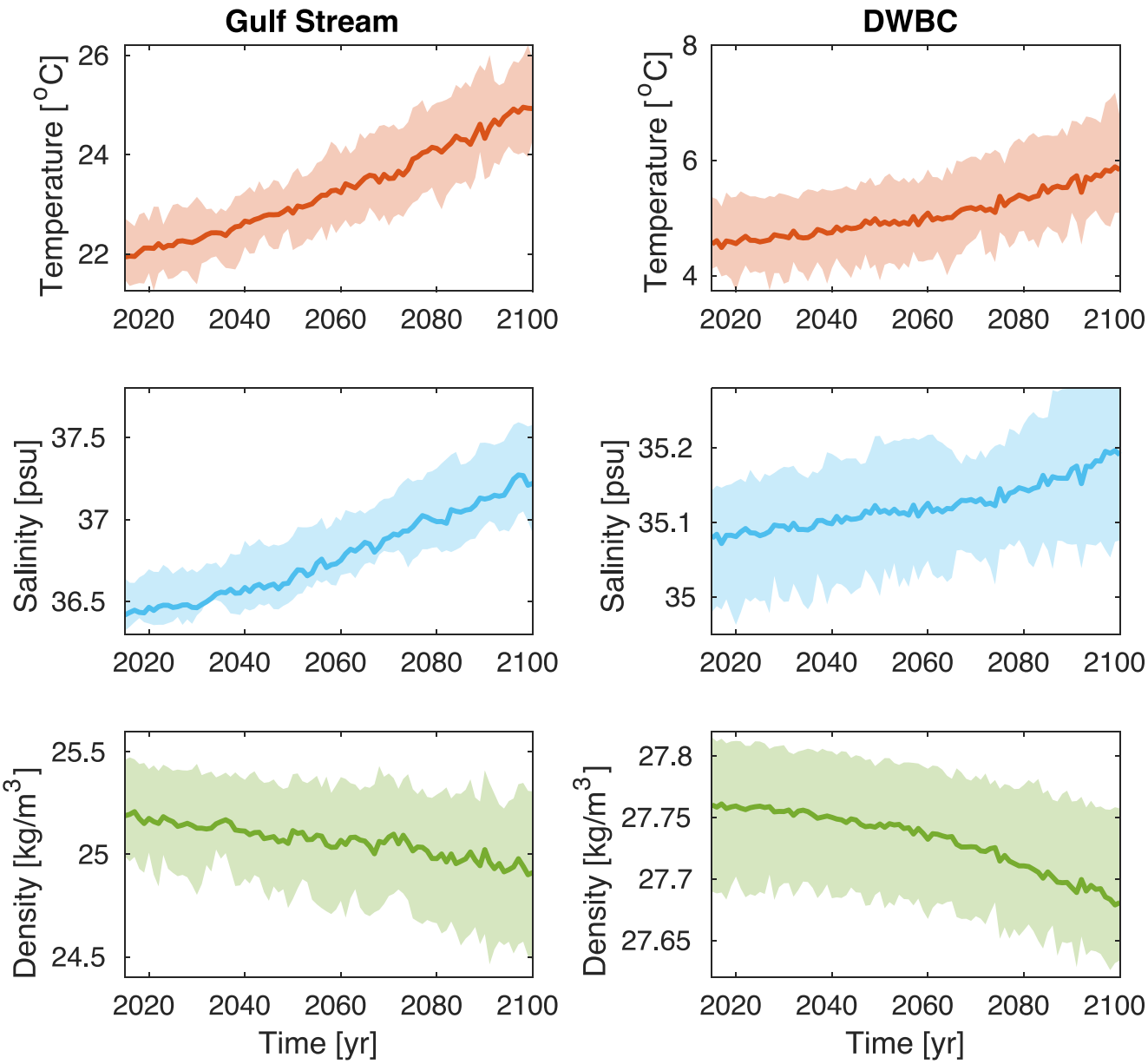

Figure 4. Time evolution of the western boundary currents' properties. Multi-model mean potential temperature, salinity, potential density for 12 models under ssp585 with interquartile range in shadings. The properties have been averaged over the Gulf Stream and DWBC cores prior to taking the multi-model mean.

Atlantic Current (Sein et al., 2018), are not necessarily well represented in coarse resolution climate models. While these caveats somewhat limit the confidence in the projections of future North Atlantic circulation, the models are still invaluable for understanding dynamical relationships between different circulation components under external forcing. The one model with higher nominal resolution (MPI-ESM1-2-HR; 0.4° × 0.4°) does not show notably different temporal evolution than the other models, suggesting that the results are not particularly sensitive to resolution.

The projected slowdown of ocean circulation and the associated reduction in northward heat transport detailed in this study could have global and regional climatic implications (Bellomo et al., 2021; Jackson et al., 2015; Liu et al., 2020). A weaker Gulf Stream is, for example, dynamically linked to sea level rise along the U.S. East Coast increasing the risk for flooding events (Ezer et al., 2013). While there is considerable inter-model spread in the projected weakening, none of the models show a collapse in any of the circulation branches. We find that the Gulf Stream, reflecting both the gyre circulation and the overturning circulation, to a larger extent is maintained

by winds in the future (Figure S6 in Supporting Information S1) ensuring a level of robustness to the circulation system.

Data Availability Statement

The CMIP6 models used in this study are listed in Table S1 in Supporting Information S1. The CMIP6 data can be downloaded from the Earth System Grid Federation (ESGF) at https://esgf-node.llnl.gov/projects/cmip6/. The RAPID-MOCHA-WBTS observational data (Moat et al., 2022) is available at https://doi.org/10.5285/e91b10af-6f0a-7fa7-e053-6c86abc05a09.

Acknowledgments
We acknowledge the World Climate Research Programme's Working Group on Coupled Modelling, which is responsible for CMIP, and we thank the individual climate modeling groups for producing and making available their model output. We also thank Anaïs Bretones and the Bjerknes Centre's DYNASOR project for useful discussions on analysis of CMIP6 models. We acknowledge the teams behind the RAPID-MOCHA-WBTS TMA projects for collecting and making data from 26.5°N freely available.

References

Årthun, M., Onarheim, I. H., Dörr, J., & Eldevik, T. (2021). The seasonal and regional transition to an ice-free Arctic. *Geophysical Research Letters*, *48*(1), e2020GL090825. https://doi.org/10.1029/2020GL090825

Baringer, M. O., & Larsen, J. C. (2001). Sixteen years of Florida current transport at 27°N. *Geophysical Research Letters*, *28*(16), 3179–3182. https://doi.org/10.1029/2001GL013246

Beadling, R. L., Russell, J. L., Stouffer, R. J., & Goodman, P. J. (2018). Evaluation of subtropical North Atlantic Ocean circulation in CMIP5 models against the observational array at 26.5°N and its changes under continued warming. *Journal of Climate*, *31*(23), 9697–9718. https://doi.org/10.1175/JCLI-D-17-0845.1

Bellomo, K., Angeloni, M., Corti, S., & von Hardenberg, J. (2021). Future climate change shaped by inter-model differences in Atlantic meridional overturning circulation response. *Nature Communications*, *12*(1), 3659. https://doi.org/10.1038/s41467-021-24015-w

Biló, T. C., & Johns, W. E. (2020). The deep western boundary current and adjacent interior circulation at 24°–30°N: Mean structure and mesoscale variability. *Journal of Physical Oceanography*, *50*(9), 2735–2758. https://doi.org/10.1175/JPO-D-20-0094.1

Bretones, A., Nisancioglu, K. H., Jensen, M. F., Brakstad, A., & Yang, S. (2022). Transient increase in Arctic deep-water formation and ocean circulation under sea-ice retreat. *Journal of Climate*, *35*(1), 109–124. https://doi.org/10.1175/JCLI-D-21-0152.1

Bryden, H. L. (2021). Wind-driven and buoyancy-driven circulation in the subtropical North Atlantic Ocean. *Proceedings of the Royal Society A*, *477*(2256). https://doi.org/10.1098/rspa.2021.0172

Cunningham, S. A., Kanzow, T., Rayner, D., Baringer, M. O., Johns, W. E., Marotzke, J., et al. (2007). Temporal variability of the Atlantic meridional overturning circulation at 26.5°N. *Science*, *317*(5840), 935–937. https://doi.org/10.1007/s10584-006-9153-z

de Coëtlogon, G., Frankignoul, C., Bentsen, M., Delon, C., Haak, H., Masina, S., & Pardaens, A. (2006). Gulf Stream variability in five oceanic general circulation models. *Journal of Physical Oceanography*, *36*(11), 2119–2135. https://doi.org/10.1175/JPO2963.1

Eden, C., & Willebrand, J. (2001). Mechanism of interannual to decadal variability of the North Atlantic circulation. *Journal of Climate*, *14*(10), 2266–2280. https://doi.org/10.1175/1520-0442(2001)014⟨2266:MOITDV⟩2.0.CO;2

Eyring, V., Bony, S., Meehl, G. A., Senior, C. A., Stevens, B., Stouffer, R. J., & Taylor, K. E. (2016). Overview of the Coupled Model Intercomparison Project Phase 6 (CMIP6) experimental design and organization. *Geoscientific Model Development*, *9*(5), 1937–1958. https://doi.org/10.5194/gmd-9-1937-2016

Ezer, T., Atkinson, L. P., Corlett, W. B., & Blanco, J. L. (2013). Gulf Stream's induced sea level rise and variability along the U.S. mid-Atlantic coast. *Journal of Geophysical Research: Oceans*, *118*(2), 685–697. https://doi.org/10.1002/jgrc.20091

Gidden, M. J., Riahi, K., Smith, S. J., Fujimori, S., Luderer, G., Kriegler, E., et al. (2019). Global emissions pathways under different socioeconomic scenarios for use in CMIP6: A dataset of harmonized emissions trajectories through the end of the century. *Geoscientific Model Development*, *12*(4), 1443–1475. https://doi.org/10.5194/gmd-12-1443-2019

Grise, K. M., & Davis, S. M. (2020). Hadley cell expansion in CMIP6 models. *Atmospheric Chemistry and Physics*, *20*(9), 5249–5268. https://doi.org/10.5194/acp-20-5249-2020

Harvey, B. J., Cook, P., Shaffrey, L. C., & Schiemann, R. (2020). The response of the northern hemisphere storm tracks and jet streams to climate change in the CMIP3, CMIP5, and CMIP6 climate models. *Journal of Geophysical Research: Atmospheres*, *125*(23), e2020JD032701. https://doi.org/10.1029/2020JD032701

Heuzé, C. (2021). Antarctic bottom water and North Atlantic deep water in CMIP6 models. *Ocean Science*, *17*(1), 59–90. https://doi.org/10.5194/os-17-59-2021

Heuzé, C., & Årthun, M. (2019). The Atlantic inflow across the Greenland-Scotland ridge in global climate models (CMIP5). *Elementa Science of the Anthropocene*, *7*, 16. https://doi.org/10.1525/elementa.354

Jackson, L. C., Kahana, R., Graham, T., Ringer, M. A., Woollings, T., Mecking, J. V., & Wood, R. A. (2015). Global and European climate impacts of a slowdown of the AMOC in a high resolution GCM. *Climate Dynamics*, *45*(11–12), 3299–3316. https://doi.org/10.1007/s00382-015-2540-2

Kanzow, T., Send, U., & McCartney, M. (2008). On the variability of the deep meridional transports in the tropical North Atlantic. *Deep Sea Research Part I: Oceanographic Research Papers*, *55*(12), 1601–1623. https://doi.org/10.1016/J.DSR.2008.07.011

Larson, S. M., Buckley, M. W., & Clement, A. C. (2020). Extracting the buoyancy-driven Atlantic meridional overturning circulation. *Journal of Climate*, *33*(11), 4697–4714. https://doi.org/10.1175/JCLI-D-19-0590.1

Levang, S. J., & Schmitt, R. W. (2020). What causes the AMOC to weaken in CMIP5? *Journal of Climate*, *33*(4), 1535–1545. https://doi.org/10.1175/JCLI-D-19-0547.1

Lique, C., & Thomas, M. D. (2018). Latitudinal shift of the Atlantic Meridional Overturning Circulation source regions under a warming climate. *Nature Climate Change*, *8*(11), 1013–1020. https://doi.org/10.1038/s41558-018-0316-5

Liu, W., Fedorov, A. V., Xie, S.-P., & Hu, S. (2020). Climate impacts of a weakened Atlantic meridional overturning circulation in a warming climate. *Science Advances*, *6*(26), eaaz4876. https://doi.org/10.1126/sciadv.aaz4876

Lozier, M. S. (2012). Overturning in the North Atlantic. *Annual Review of Marine Science*, *4*(1), 291–315. https://doi.org/10.1146/annurev-marine-120710-100740

Lu, J., Vecchi, G. A., & Reichler, T. (2007). Expansion of the Hadley cell under global warming. *Geophysical Research Letters*, *34*(6), L06805. https://doi.org/10.1029/2006GL028443

Maroon, E. A., Kay, J. E., & Karnauskas, K. B. (2018). Influence of the Atlantic meridional overturning circulation on the northern hemisphere surface temperature response to radiative forcing. *Journal of Climate*, *31*(22), 9207–9224. https://doi.org/10.1175/JCLI-D-17-0900.1

Meinen, C. S., Johns, W. E., Moat, B. I., Smith, R. H., Johns, E. M., Rayner, D., et al. (2019). Structure and variability of the Antilles current at 26.5°N. *Journal of Geophysical Research: Oceans*, *124*(6), 3700–3723. https://doi.org/10.1029/2018JC014836

Menary, M. B., Robson, J., Allan, R. P., Booth, B. B. B., Cassou, C., Gastineau, G., et al. (2020). Aerosol-forced AMOC changes in CMIP6 historical simulations. *Geophysical Research Letters*, *47*(14), e2020GL088166. https://doi.org/10.1029/2020GL088166

Moat, B. I., Frajka-Williams, E., Rayner, D., Johns, W. E., Baringer, M. O., Volkov, D. L., & Collins, J. (2022). Atlantic meridional overturning circulation observed by the RAPID-MOCHA-WBTS array at 26N from 2004 to 2020 (v2020.2) [Dataset]. NERC EDS British Oceanographic Data Centre NOC. https://doi.org/10.5285/e91b10af-6f0a-7fa7-e053-6c86abc05a09

Moat, B. I., Smeed, D. A., Frajka-Williams, E., Desbruyères, D. G., Beaulieu, C., Johns, W. E., et al. (2020). Pending recovery in the strength of the meridional overturning circulation at 26N. *Ocean Science*, *16*(4), 863–874. https://doi.org/10.5194/os-16-863-2020

Østerhus, S., Woodgate, R., Valdimarsson, H., Turrell, B., de Steur, L., Quadfasel, D., et al. (2019). Arctic Mediterranean exchanges: A consistent volume budget and trends in transports from two decades of observations. *Ocean Science*, *15*(2), 379–399. https://doi.org/10.5194/os-15-379-2019

Robson, J., Menary, M. B., Sutton, R. T., Mecking, J., Gregory, J. M., Jones, C., et al. (2022). The role of anthropogenic aerosol forcing in the 1850–1985 strengthening of the AMOC in CMIP6 historical simulations. *Journal of Climate*, *35*(20), 3243–3263. https://doi.org/10.1175/JCLI-D-22-0124.1

Roquet, F., & Wunsch, C. (2022). The Atlantic meridional overturning circulation and its hypothetical collapse. *Tellus A: Dynamic Meteorology and Oceanography*, *74*(1), 393–398. https://doi.org/10.16993/tellusa.679

Sein, D. V., Koldunov, N. V., Danilov, S., Sidorenko, D., Wekerle, C., Cabos, W., et al. (2018). The relative influence of atmospheric and oceanic model resolution on the circulation of the North Atlantic Ocean in a coupled climate model. *Journal of Advances in Modeling Earth Systems*, *10*(8), 2026–2041. https://doi.org/10.1029/2018MS001327

Sen Gupta, A., Stellema, A., Pontes, G. M., Taschetto, A. S., Vergés, A., & Rossi, V. (2021). Future changes to the upper ocean Western Boundary Currents across two generations of climate models. *Scientific Reports*, *11*(1), 9538. https://doi.org/10.1038/s41598-021-88934-w

Sverdrup, H. U. (1947). Wind-driven currents in a baroclinic ocean; with application to the equatorial currents of the eastern Pacific. *Proceedings of the National Academy of Sciences of the United States of America*, *33*(11), 318–326. https://doi.org/10.1073/pnas.33.11.318

Swingedouw, D., Houssais, M.-N., Herbaut, C., Blaizot, A.-C., Devilliers, M., & Deshayes, J. (2022). AMOC recent and future trends: A crucial role for oceanic resolution and Greenland melting? *Frontiers in Climate*, *4*, 838310. https://doi.org/10.3389/fclim.2022.838310

Thomas, M. D., De Boer, A. M., Johnson, H. L., & Stevens, D. P. (2014). Spatial and temporal scales of Sverdrup balance. *Journal of Physical Oceanography*, *44*(10), 2644–2660. https://doi.org/10.1175/JPO-D-13-0192.1

Thomas, M. D., de Boer, A. M., Stevens, D. P., & Johnson, H. L. (2012). Upper ocean manifestations of a reducing meridional overturning circulation. *Geophysical Research Letters*, *39*(16), L16609. https://doi.org/10.1029/2012GL052702

Weaver, A. J., Sedláček, J., Eby, M., Alexander, K., Crespin, E., Fichefet, T., et al. (2012). Stability of the Atlantic meridional overturning circulation: A model intercomparison. *Geophysical Research Letters*, *39*(20), 2012GL053763. https://doi.org/10.1029/2012GL053763

Weijer, W., Cheng, W., Garuba, O. A., Hu, A., & Nadiga, B. T. (2020). CMIP6 models predict significant 21st century decline of the Atlantic meridional overturning circulation. *Geophysical Research Letters*, *47*(12), e2019GL086075. https://doi.org/10.1029/2019GL086075

Wunsch, C., & Heimbach, P. (2013). Two decades of the Atlantic meridional overturning circulation: Anatomy, variations, extremes, prediction, and overcoming its limitations. *Journal of Climate*, *26*(18), 7167–7186. https://doi.org/10.1175/JCLI-D-12-00478.1

Yang, H., Lohmann, G., Krebs-Kanzow, U., Ionita, M., Shi, X., Sidorenko, D., et al. (2020). Poleward shift of the major ocean gyres detected in a warming climate. *Geophysical Research Letters*, *47*(5), e2019GL085868. https://doi.org/10.1029/2019GL085868

References From the Supporting Information

Boucher, O., Servonnat, J., Albright, A. L., Aumont, O., Balkanski, Y., Bastrikov, V., et al. (2020). Presentation and evaluation of the IPSL-CM6A-LR climate model. *Journal of Advances in Modeling Earth Systems*, *12*(7), e2019MS002010. https://doi.org/10.1029/2019MS002010

Döscher, R., Acosta, M., Alessandri, A., Anthoni, P., Arsouze, T., Bergman, T., et al. (2022). The EC-Earth3 Earth system model for the coupled model intercomparison project 6. *Geoscientific Model Development*, *15*(7), 2973–3020. https://doi.org/10.5194/gmd-15-2973-2022

Kelley, M., Schmidt, G. A., Nazarenko, L. S., Bauer, S. E., Ruedy, R., Russell, G. L., et al. (2020). GISS-E2.1: Configurations and climatology. *Journal of Advances in Modeling Earth Systems*, *12*(8), e2019MS002025. https://doi.org/10.1029/2019MS002025

Lovato, T., Peano, D., Butenschön, M., Materia, S., Iovino, D., Scoccimarro, E., et al. (2022). CMIP6 simulations with the CMCC Earth system model (CMCC-ESM2). *Journal of Advances in Modeling Earth Systems*, *14*(3), e2021MS002814. https://doi.org/10.1029/2021MS002814

Müller, W. A., Jungclaus, J. H., Mauritsen, T., Baehr, J., Bittner, M., Budich, R., et al. (2018). A higher-resolution version of the Max Planck institute Earth system model (MPI-ESM1.2-HR). *Journal of Advances in Modeling Earth Systems*, *10*(7), 1383–1413. https://doi.org/10.1029/2017MS001217

Séférian, R., Nabat, P., Michou, M., Saint-Martin, D., Voldoire, A., Colin, J., et al. (2019). Evaluation of CNRM Earth system model, CNRM-ESM2-1: Role of Earth system processes in present-day and future climate. *Journal of Advances in Modeling Earth Systems*, *11*(12), 4182–4227. https://doi.org/10.1029/2019MS001791

Seland, Y., Bentsen, M., Olivié, D., Toniazzo, T., Gjermundsen, A., Graff, L. S., et al. (2020). Overview of the Norwegian Earth System Model (NorESM2) and key climate response of CMIP6 DECK, historical, and scenario simulations. *Geoscientific Model Development*, *13*(12), 6165–6200. https://doi.org/10.5194/gmd-13-6165-2020

Sellar, A. A., Walton, J., Jones, C. G., Wood, R., Abraham, N. L., Andrejczuk, M., et al. (2020). Implementation of U.K. Earth system models for CMIP6. *Journal of Advances in Modeling Earth Systems*, *12*(4), e2019MS001946. https://doi.org/10.1029/2019MS001946

Swart, N. C., Cole, J. N. S., Kharin, V. V., Lazare, M., Scinocca, J. F., Gillett, N. P., et al. (2019). The Canadian Earth system model version 5 (CanESM5.0.3). *Geoscientific Model Development*, *12*(11), 4823–4873. https://doi.org/10.5194/gmd-12-4823-2019

Tatebe, H., Ogura, T., Nitta, T., Komuro, Y., Ogochi, K., Takemura, T., et al. (2019). Description and basic evaluation of simulated mean state, internal variability, and climate sensitivity in MIROC6. *Geoscientific Model Development*, *12*(7), 2727–2765. https://doi.org/10.5194/gmd-12-2727-2019

Wu, T., Lu, Y., Fang, Y., Xin, X., Li, L., Li, W., et al. (2019). The Beijing climate center climate system model (BCC-CSM): The main progress from CMIP5 to CMIP6. *Geoscientific Model Development*, *12*(4), 1573–1600. https://doi.org/10.5194/gmd-12-1573-2019

Yukimoto, S., Kawai, H., Koshiro, T., Oshima, N., Yoshida, K., Urakawa, S., et al. (2019). The meteorological research institute Earth system model version 2.0, MRI-ESM2.0: Description and basic evaluation of the physical component. *Journal of the Meteorological Society of Japan*, *97*(5), 931–965. https://doi.org/10.2151/jmsj.2019-051

Ziehn, T., Chamberlain, M. A., Law, R. M., Lenton, A., Bodman, R. W., Dix, M., et al. (2020). The Australian Earth system model: ACCESS-ESM1.5. *Journal of Southern Hemisphere Earth Systems Science*, *70*(1), 193–214. https://doi.org/10.1071/ES19035